ARTICLES

Al K-Edge Near-Edge X-ray Absorption Fine Structure (NEXAFS) Study on the Coordination Structure of Aluminum in Minerals and Y Zeolites

J. A. van Bokhoven,† H. Sambe,† D. E. Ramaker,† and D. C. Koningsberger*,‡

Chemistry Department, George Washington University, Washington, D.C. 20052 and Laboratory of Inorganic Chemistry and Catalysis, Debye Institute, Utrecht University, 3508 TB Utrecht, The Netherlands

Received: February 9, 1999; In Final Form: June 21, 1999

Curved-wave−multiple-scattering cluster calculations with the FEFF6 code were used to interpret experimental AlK-edge near-edge X-ray absorption fine structure (NEXAFS) spectra of various minerals and Y zeolites for energies ∼15 eV above threshold. Octahedral, tetrahedral, and square planar geometries of Al can be easily distinguished from each other utilizing characteristic features in the NEXAFS data. NEXAFS line shapes are used for determining the geometrical conformations of Al atoms in Y zeolites with one or more conformational geometries. In the H−Y zeolite, separate contributions to the NEXAFS from tetrahedrally and octahedrally coordinated Al atoms are identified. The differences in the octahedrally coordinated Al spectra in the H−Y zeolite compared with spectra for standard octahedrally coordinated Al compounds can be attributed to the presence of very small nonregular clusters of octahedrally coordinated Al dispersed over the zeolite. However, the presence of some pentacoordinated Al cannot be excluded.

Introduction

Zeolites are widely used as catalysts and as catalyst supports in industrial processes. Applications can be found in processes such as fluid catalytic cracking, hydro-cracking, paraffin isomerization, aromatic alkylation, ion-exchange resins, molecular sieves, sorbents etc.[1−3] Zeolites are open framework aluminosilicates consisting of SiO_4^{-4} and AlO_4^{-5} tetrahedra, interconnected via the oxygen atoms. Charge balance requires the presence of one cation for each Al atom. These cations are not part of the framework and can easily be exchanged.[4] Physical properties, like the catalytic activity, are primarily determined by the structure of the zeolite, the presence of extraframework species, etc. Although zeolites have been under investigation for many years, no clear relationship between local and electronic structure and activity has been established.[5] For example, the influence of the extraframework Al species on the catalytic activity is still unclear and even the exact structure of the extraframework Al species is not known. Clearly, detailed structural investigations of Al species in zeolites are needed.

We present here X-ray absorption spectroscopy (XAFS) studies on the AlK-edge. XAFS spectroscopy is a very useful technique for probing the local atomic environment of different substituents in a material. Application of this technique is widespread, and the material to be studied can be either a gas, a liquid, or a solid, because long-range structure is not required. Extended X-ray absorption fine structure (EXAFS) analysis yields the coordination number, bond distances, type of neighbors, and the local disorder. Near-edge X-ray absorption fine structure (NEXAFS) can provide additional information on the coordination geometry, the symmetry of the unoccupied states, and the effective atomic charge on the absorbing atom.[6]

Previous analysis of the EXAFS data for the Y zeolite with different cations (H^+, NH_4^+, and Na^+) indicated that these three materials have slightly different Al−O bond lengths and possess primarily 4-fold (probably tetrahedrally) coordinated Al sites.[7] The previously published NEXAFS data are analyzed in detail in this work.

In this paper we demonstrate the usefulness of NEXAFS data for the determination of the local Al environment in minerals and Y zeolites. The Al coordinations we consider are the tetrahedral (undistorted and distorted), the square planar, and the octahedral. We perform curved-wave multiple-scattering calculations with the FEFF6 code on various clusters representing the mineral or zeolite. The calculated results are compared with the experimental AlK-edge NEXAFS data from a wide array of aluminum oxide minerals. Some of these data are taken from the literature. From these comparisons, we recognize characteristic features or "fingerprints" in the spectra arising from the different Al coordination geometries.

After establishing the characteristic features that allow distinctions between the Al coordinations, we analyze the NEXAFS range of the Y zeolite absorption spectra just mentioned. A technique to separate the different contributions from different Al coordinations in a NEXAFS spectrum is described. Although some part of this work has been briefly reported,[8] we provide here the full analysis and results.

Experimental and Theoretical Methods

Experimental spectra are compared on an energy scale relative to the maximum or shoulder of the first intense peak (whiteline)

* Corresponding author. Telephone: +31-30-253-74-00. Fax: +31-30-2511-027. E-mail: d.c.koningsberger@chem.uu.nl.
† Chemistry Department.
‡ Laboratory of Inorganic Chemistry and Catalysis.

10.1021/jp990478t CCC: $18.00
Published on Web 08/20/1999

in the spectra. This comparison meant a shift of, on average, 1568 eV for tetrahedrally coordinated Al, and 1570 and 1572 eV for distorted and regular octahedral, respectively, in Perovskite. These AlK-edge XAFS spectra of the Y zeolites were taken at the soft X-ray XAFS station 3.4 of the Synchrotron Radiation Source at Daresbury (UK). Experimental details have been published elsewhere.[7] Standard procedures were used to analyze the data.[9] Briefly, the data were normalized to 1 at 50 eV above the edge, and the postedge background was subtracted using cubic spline routines.[10] All experimental spectra presented in this study were obtained using total electron yield detection (TEY).

Curved-wave−multiple-scattering (CW−MS) cluster calculations utilizing the FEFF6 code developed by Rehr and Albers[11,12] were performed in this work. We have previously[13,14] performed FEFF6 calculations on alkali halides and condensed rare gases to test the validity of this code and found that the code reproduces almost all of the experimentally observed peaks except the highly localized excitonic peaks very near or below the edge (particularly for Ne). For the first row transition metals and lighter elements, the absolute energy must be shifted by 0−5 eV for optimum agreement with experimentally observed results. Here, the FEFF6 results were optimally aligned with the experimental data. The theoretical spectra were also normalized at 50 eV above the edge.

The input parameters for the theoretical calculations include the atomic number of each unique atom in the cluster, the coordinates of each atom in the cluster, the choice of exchange potential (Hedin−Lundquest, Dirac−Hara, or ground state), the maximum path length, criteria for the path filter that determines the amount of multiple scattering, the Debye−Waller factor (σ^2), and the charge on the ions. We employed the ground-state exchange-correlated potential, which does not allow for inelastic energy losses. We used a zero imaginary part in the potential, thus ignoring any lifetime and experimental broadening effects. The maximum path length was set to 8−10 Å for the 1 and 2 shell calculations, and to 15 Å for the 7 shell calculations. The path filter was chosen to be 1% for the plane waves and 2% for the curved waves (i.e., 1/2 of the default values) to include all-important multiple scattering paths. The Debye−Waller factor was set to 0.007 Å^2.

Results and Discussion

Octahedral Coordination. Experimental AlK-edge NEXAFS data for aluminum oxide compounds with an octahedral coordination are given in Figures 1 and 2. Figure 1 gives results over an extended range, 0−50, and Figure 2 emphasizes the whiteline region, 0−15 eV. Basically, the features can be divided into three regions: the whiteline region (0−15 eV), the intermediate region (15−40 eV), and the high-energy region (40−55 eV). In Figure 1, experimental data are given for the compounds that exhibit the Perovskite structure (1 = $YAlO_3$, 2 = $NdAlO_3$) with a nondistorted octahedral Al coordination.[15] FEFF6 multiple-scattering calculated results for a single-shell AlO_6 cluster with the symmetric Perovskite structure with an Al−O bond length of 1.92 Å are also given. Finally, FEFF6 multiple-scattering results for an $Al_{15}O_{18}^{-10}$ cluster with the crystal structure of corundum, a distorted octahedral, are shown.

All spectra, the single- and multi-shell FEFF6 results, regardless of local symmetry, and the experimental data, reveal essentially the same feature in the 40−55 eV region. These results very strongly suggest that this feature arises from Al−O single EXAFS scattering, which is confirmed by analyzing the scattering paths that indicate that this feature has its origin in single scattering. As such, this feature should be highly dependent on the Al−O bond length. A small energy shift does exist between the two FEFF6 spectra, which arises from the different bond lengths utilized in the calculations. The corundum structure has two different Al−O bond lengths (1.86 and 1.97 Å, respectively[16]), but only one peak is visible in the calculated spectra in this region.

The set of small features (appearing almost as 4 features) around 15−40 eV in the experimental spectra, most clearly visible in Perovskite 2, are reproduced in the calculated spectrum by two broader peaks. Adding countercations (Nd) and including more shells (up to 7 shells) in the calculation does not result in

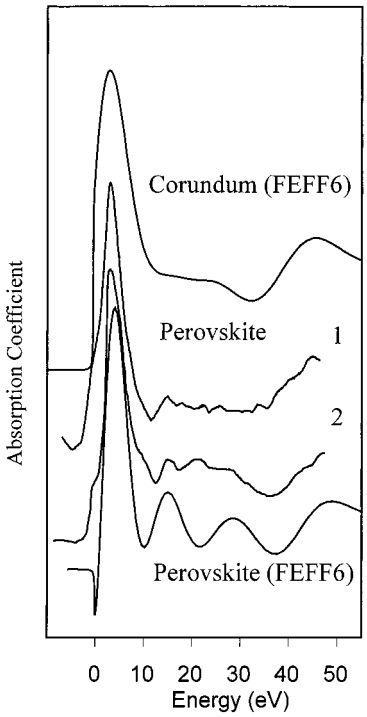

Figure 1. Experimental NEXAFS data for two different perovskites [$YAlO_3$ (1) and $NbAlO_3$ (2)[15]] with octahedral Al sites. Also shown are results from FEFF6 calculations on clusters representing nondistorted (perovskite) and distorted (corundum) Al sites.

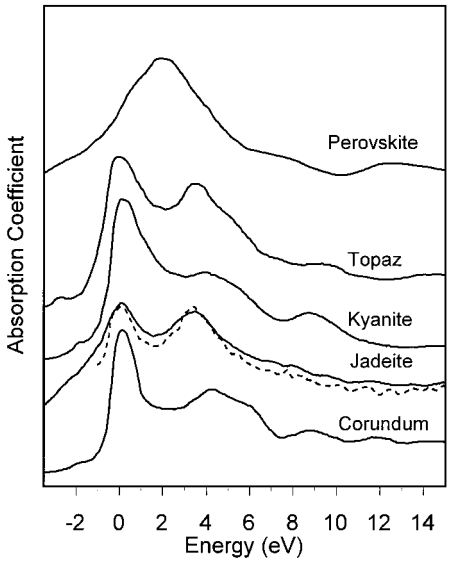

Figure 2. Experimental NEXAFS spectra for several materials possessing nondistorted octahedral or distorted octahedral Al sites; perovskite ($YAlO_3$), topaz,[17] kayanite,[17] jadeite (dotted,[17] solid[19]), and corundum[20] are shown.

the splitting of these two peaks. Experimental Al NEXAFS spectra for $KAlF_4$ and K_2NaAlF_6, which exhibit structures that are associated with the Perovskite structure, do show only two peaks around 15−40 eV.[15] Thus, the splitting of the two peaks in the experimental spectra for $NdAlO_3$ might be a result of small irregularities in these crystal structures, such as variations in bond length. These peaks between 15 and 40 eV can be assigned to Al−O σ* antibonding orbitals because they appear already in the FEFF results for a multiple-scattering calculation on a single-shell cluster, but they do not appear in a single-scattering calculation. These peaks are dependent on the local geometry because Al−O−O multiple scattering is also involved. From a molecular orbital point of view, these σ* antibonding orbitals should also depend on the local geometry.

Now, we consider the whiteline region at 0−15 eV. Figure 2 shows experimental Al NEXAFS data for materials that possess distorted octahedrally coordinated Al sites; topaz,[17,18] kyanite,[17,18] jadeite,[17,19] and corundum.[18−20] The spectrum of topaz from ref 15 was shifted about one extra electronvolt to lower energy for optimal agreement in whiteline position with the other spectra. In addition, an experimental AlK-edge NEXAFS spectrum for an undistorted octahedral Perovskite structure ($YAlO_3$) is given. The spectrum of the Perovskite structure shows a single whiteline peak, whereas the materials with distorted octahedral Al sites all show a splitting of the whiteline by ∼4 eV. It has been established in the literature[17−20] that materials with distorted octahedral Al sites have edge features at 1568 and 1572 eV, whereas the Perovskite structure, with undistorted octahedral Al sites, has a single whiteline at 1570 eV[15] (the average of these two energies). Although the magnitude of the whiteline splitting in all the distorted structures remains constant around 4 eV, the relative intensities of the two peaks vary. In addition to the split whiteline, a weak preedge feature (at ca. −2 eV) can be seen in all of the spectra of the distorted octahedral compounds.

The strong dependence of the whiteline region on the nondistorted versus distorted octahedral symmetry, suggests that the whiteline depends primarily on the local geometry; however, strong evidence exists that it also depends on the long-range structure. For example, the experimental spectrum for $KAl(SO_4)_2{\cdot}12H_2O$, in which the aluminum has a nondistorted octahedral coordination, still shows a split whiteline.[21] This result illustrates the influence of the long-range structure on the whiteline of octahedral Al.

The FEFF6 results do not reproduce the whiteline region of corundum despite the full multiple-scattering calculations on several shells. Recently, Cabaret et al.[22] calculated the AlK-edge spectrum for corundum using very large clusters (up to 15.3 Å), full multiple scattering, and the "extended continuum" code developed by Natoli et al.[23] They obtained excellent agreement with the experimental whiteline. However, for cluster diameters <11 Å, very poor agreement was found. We conclude that the whiteline in this case depends strongly on both the local geometry and the long-range structure. We assign this whiteline region to the weakly antibonding or nonbonding orbitals. Because they are more diffuse orbitals, the whiteline feature is much more dependent on the long-range structure.

Tetrahedral Coordination. Experimental Al NEXAFS spectra for structures that have tetrahedrally coordinated Al sites are given in Figure 3. The Na^+−Y and NH_4^+−Y zeolites are, respectively, 100% and 98% tetrahedrally coordinated according to ^{27}AL MAS NMR. Albite[24] is used as a reference spectrum for compounds with tetrahedrally coordinated aluminum oxide in the literature.[17,19,20] A calculated FEFF6 spectrum for an AlO_4 cluster is also shown. For this multiple-scattering calculation the cluster is in a regular tetrahedral conformation with an Al−O bond length of 1.70 Å.

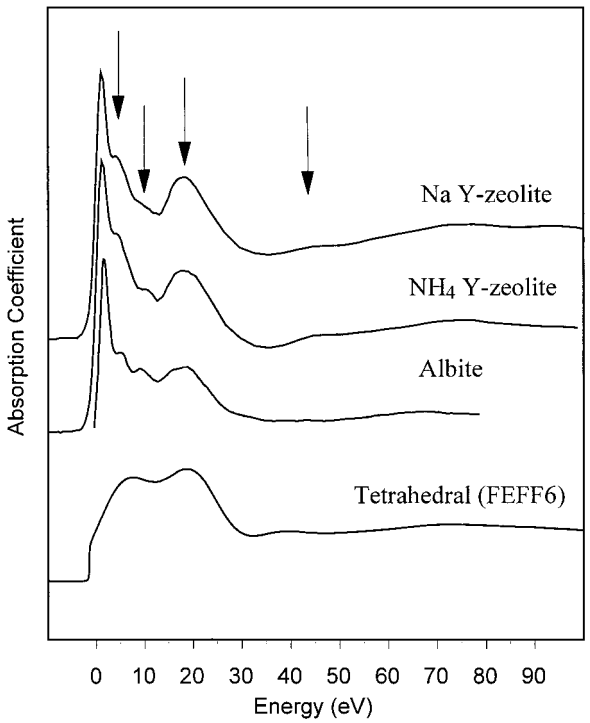

Figure 3. NEXAFS AlK-edge data for Na^+−Y and NH_4^+−Y zeolites,[7] and albite[24] (i.e., for materials with tetrahedrally coordinated Al sites). Also shown is an FEFF6 calculation on an AlO_4 cluster with tetrahedral symmetry.

The FEFF6 results on the one-shell cluster show no intensity at the edge, and the sharp whiteline, dominating the experimental spectra, is absent in the one-shell calculation. However, the one-shell calculation already reproduces the relative peak positions and intensities of the peaks around 20 and 75 eV in the experimental spectra. A small peak around 45 eV in the experimental spectra appears around 40 eV in the FEFF6 spectrum. These results are completely consistent with the octahedral assignment; that is, the 75 eV peak is assigned to Al−O single EXAFS scattering, similar to the 45 eV peak in the octahedral case. The higher energy reflects the shorter Al−O bond length in the tetrahedral case. The 20 eV peak falls in the same range as the σ* orbital in the octahedral case, and we assign it as such. Based on the position of the peak at 20 eV, which is also sensitive to the bond length, the FEFF6 calculations suggest an Al−O bond length in the range 1.70 Å for all three Y zeolites. The FEFF6 calculations also indicate that several single- and multiple-scattering paths within the first shell are responsible for this peak, which again is consistent with its σ* character.

Again, the FEFF6 calculation on a single-shell cluster does not reproduce the whiteline structure; indeed, in this tetrahedral case, a strong whiteline does not appear at all. The two peaks visible in the three experimental spectra around 5−10 eV are suggested in the FEFF6 calculated spectrum by a single peak around 8 eV. Again, Cabaret et al.[22] performed MS cluster calculations on large clusters (up to 15.7 Å) and reproduced all the features in this 0−15 eV range. The whiteline region again appears to depend on both local geometry and long-range structure, which is consistent with a weakly antibonding or nonbonding, and more diffuse, molecular orbital assignment.

Square Planar and Other Coordinations. Experimental and FEFF6 spectra for structures in which the absorber atom has a

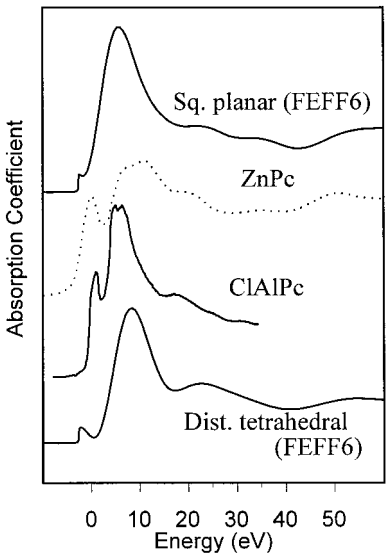

Figure 4. NEXAFS K-edge data for a square planar coordination, ClAlPc (AlK-edge)[25] and ZnPc (Zn K-edge). Also shown is an FEFF6 calculation for an AlO_4 cluster with square planar symmetry.

square planar conformation are given in Figure 4. Experimental ZnK-edge data for zinc phthalocyanine, and AlK-edge data for chloroaluminum phthalocyanine[25] are given. Both structures are reported to have a square planar coordination of, respectively, the Z and Al atoms. FEFF6 calculations for an AlO_4 cluster in a square planar coordination with M−O bond length of 1.70 Å are also shown. The experimental spectra, although quite different, have similar features. Both reveal a large characteristic preedge peak (so-called because of its appearance prior to the main whiteline feature), which arises from the nonbonding p_z orbital perpendicular to the plane in the square planar coordination.

The FEFF6 results show similarities with the experimental spectra, even though the absorber atom and the backscattering atoms assumed in the calculations are different from those in the experimental materials. The preedge peak is highly underestimated in the FEFF6 results, as expected, because the FEFF6 code has difficulty reproducing localized states.[13]

Except for the preedge feature, the spectra for structures with a square planar conformation show similarities with spectra for structures with an octahedral conformation (Figure 1). This result is not surprising because the square planar conformation can be seen as an octahedral coordination after removal of any two diametrically positioned oxygen atoms.

In addition to calculations on tetrahedral and square planar clusters, we performed FEFF6 calculations on four coordinated clusters with a structure that is roughly an average between the tetrahedral and square planar coordinations. The distortions from the tetrahedral structure can be seen as a twist of two oxygen atoms over 45° along the shortest route to the square planar coordination. The Al−O bond length in this cluster is 1.67 Å. The resultant NEXAFS spectrum, given in Figure 4, shows a 50% decrease in intensity in the range 5−15 eV compared with spectra for tetrahedrally coordinated sites. The peak around 20 eV visible in the spectra of tetrahedrally coordinated compounds, is now completely absent. A broad feature around 65−70 eV appears, which is characteristic of the average Al−O bond length distance assumed in this calculation.

Comparison of Spectra for Tetrahedral and Octahedral Coordinations. Comparison of Figures 1, 2, and 3 reveal that the AlK-edge NEXAFS spectra for aluminum oxide minerals with (distorted) octahedral coordination, like jadeite, corundum, topaz, and kyanite, exhibit strong edge features at 1568 and 1572 eV. In contrast, structures with the Perovskite (regular octahedral) structure show one strong feature at about 1570 eV. Spectra for aluminum oxide minerals with tetrahedral coordination, like albite, show one strong edge feature at 1566 eV. Other Al NEXAFS spectra for aluminum oxide minerals with the Al in a tetrahedral coordination, like nepheline[19,22] (not shown here), also exhibit one strong edge feature at 1566 eV. Thus, there is a shift of 2 eV to lower energy for tetrahedral aluminum in comparison with the first feature in the distorted octahedrally coordinated aluminum sites.

In addition to this whiteline shift, an increase in whiteline intensity can be observed when the octahedrally coordinated sites are dominant. To check this phenomenon of higher whiteline intensity for octahedrally coordinated Al sites, we compared the ratio of the whiteline intensity to the intensity of the spectrum well above threshold for several octahedral and tetrahedral compounds. All cases in the literature (compare spectra in Figures 1 and 3) reveal a higher ratio for the octahedral compounds. It can be concluded that the NEXAFS spectra of octahedrally coordinated compounds have a higher whiteline intensity than spectra of tetrahedrally coordinated compounds.

Several criteria can now be summarized that can be used to distinguish coordinations in AlK-edge NEXAFS. These criteria are summarized in Table 1. Octahedrally coordinated Al sites can be distinguished from tetrahedrally coordinated sites in AlK-edge NEXAFS data because the whiteline shifts to higher energy and increases in intensity in the octahedral case. The longer Al−O bond length in the octahedrally coordinated compounds results in a peak at ∼40−50 eV above threshold, whereas the shorter bond length in the tetrahedral compounds gives a peak at ∼60−75 eV above threshold, which is a strong variation with bond length in this EXAFS feature. Moreover, the tetrahedral compounds show a strong feature at ∼20 eV above threshold; the corresponding feature is much weaker in the octahedral compounds because of the inversion symmetry present in the octahedral compounds. Obviously, these σ^* peaks in the NEXAFS spectra are also bond length dependent (although less so than the EXAFS features) as confirmed by FEFF6 calculations.

Distorted octahedral sites show a doublet whiteline in NEXAFS spectra. The fine structure within the whitelines in the distorted octahedral and tetrahedral coordinations is the result of long-range order. Different distortions lead to variations in intensity of the two peaks, whereas their positions remain fixed.

Preedge features appear in the distorted and square planar coordinations. These preedge features are the result of splitting of the p orbitals due to an asymmetric environment in these coordinations.

Y Zeolite Al NEXAFS. In Figure 5, the AlK-edge NEXAFS spectra for the Y zeolite with, respectively, H^+, NH_4^+, and Na^+ as cations, are given. Also the differences between the H^+−Y data and the NH_4^+ and Na^+−Y data (dif. NH_4−Y and dif. Na−Y, respectively) are shown. The EXAFS analysis on these three samples yielded the following bond lengths, coordination numbers, and Debye−Waller factors: $R = 1.700$ Å, $N = 4.4$, $\Delta\sigma^2 = 0.003$ Å for H^+−Y, $R = 1.636$ Å, $N = 4.2$, $\Delta\sigma^2 = 0.003$ Å for NH_4^+−Y, and $R = 1.620$ Å, $N = 3.8$, $\Delta\sigma^2 = -0.005$ Å for Na^+−Y. The accuracy based on a full statistical analysis of the data is ±0.003 Å for distances, ±0.1 for coordination number, and ±0.001 Å^2 for Debye−Waller factors. The EXAFS data analysis further indicates that in each sample only one Al−O bond length could be detected.[7] The data

TABLE 1: Criteria that Can Be Used to Distinguish Coordinations in AlK-Edge NEXAFS Spectra

coordination	edge position (eV)	whiteline intensity	split whiteline (eV)	characteristic peaks (eV)[a]	preedge
tetrahedral	1566	low	yes	20 and 70	no
octahedral[b]	1570	high	no	50	no
distorted octahedral	1568	high	4	50	small
square planar	XXX	medium	no	XXX	large

[a] Indicative of Al−O bond length. [b] As in Perovskite structures.

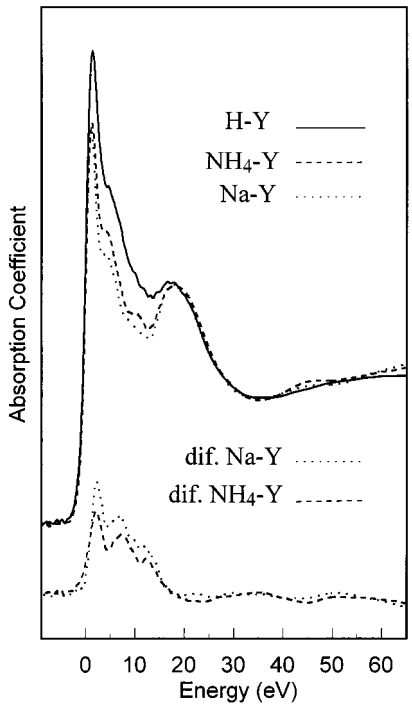

Figure 5. Comparison of AlK-edge NEXAFS data for H^+-Y, NH_4^+-Y, and Na^+-Y zeolites treated as described earlier.[7] The difference (dif.) spectra represent Na^+-Y minus H^+-Y and NH_4^+-Y minus H^+-Y, respectively.

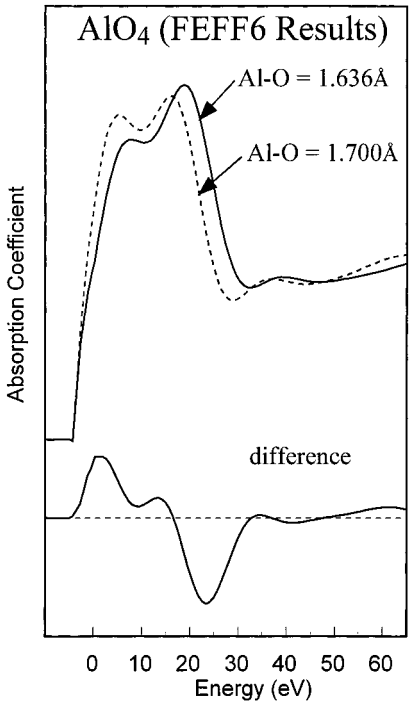

Figure 6. FEFF6 results for the AlK-edge on AlO_4 clusters for two different Al−O bond lengths. The difference, long (1.70 Å) minus short (1.636 Å) distance, between these two spectra is also shown.

analysis is impeded by the short data range that can be used to generate Al EXAFS in this work, which can result in a strong correlation between fit parameters (e.g., between N and $\Delta\sigma^2$). It will be shown later that NEXAFS analysis can give complementary information.

To study in more detail any geometric effects in these samples, we investigated the influence of differences in the Al−O bond length and of the presence of a cation in the second coordination shell of the Al atoms. We have established that the FEFF6 code is able to reproduce experimental AlK-edge spectra quite accurately above 10 eV, so it is reasonable to use FEFF6 calculations to investigate these geometric influences.

Influence of Bond Length and Monovalent Cations on Tetrahedral Conformation. In Figure 6, FEFF6 calculations on tetrahedrally coordinated aluminum oxides with bond lengths of 1.700 and 1.636 Å are given. The Al−O bond length for the calculations are chosen according to EXAFS results of the H^+-Y and NH_4^+-Y zeolite spectra. Included in the figure is the difference between the two spectra. The peaks in the spectrum shift downward with increase in bond length. Therefore, the difference spectrum contains (large) positive and negative contributions, as shown in Figure 6. The larger the difference in bond length, the larger the shift of the peaks.

Because the AlK-edge whiteline is also partially determined by long-range order, the change of nearby cations could cause the differences noted in Figure 5. Spectra of tetrahedrally coordinated AlO_4 clusters with and without a N atom in the second shell are shown in Figure 7. The N atom is representing an ammonium group (NH_4^+); where hydrogen atoms are ignored because hydrogen is known not to have significant scattering power.[6] The aluminum oxygen bond length is 1.60 Å and the aluminum nitrogen bond length 2.94 Å. This value is predicted by quantum mechanical ab initio calculations on a cluster ($HAl(OH)_3NH_4$) representing zeolites.[26] Again the difference spectrum is given. Although there is a significant influence on the spectra by the cation, this influence is small in the range starting 5 eV above threshold.

By comparing all the difference spectra (dif. Na−Y, dif. NH_4-Y, and the two theoretical difference spectra) in Figures 5, 6, and 7, the following can be concluded. The large negative contributions shown in Figure 6, which are the result of differences in bond length between emitter and backscatterer, are completely absent in the dif. Na−Y and dif. NH_4-Y spectra in Figure 5. Next, the presence of a cation other then hydrogen in the second coordination shell (Figure 7) yields a negative contribution at ∼5−25 eV above threshold, the range in which the difference spectra of the Y zeolites (dif. Na−Y and dif. NH_4-Y) show a large positive contribution. Finally, the magnitudes of these calculated difference spectra are small and a factor of ∼5 less in comparison with the experimental differences found.

It can be concluded that neither differences in Al−O bond length nor the change of cations can account for the differences seen in the zeolite spectra. In the next section, we will investigate whether these differences can be explained by assuming the presence of distorted octahedrally coordinated Al in H^+-Y zeolite.

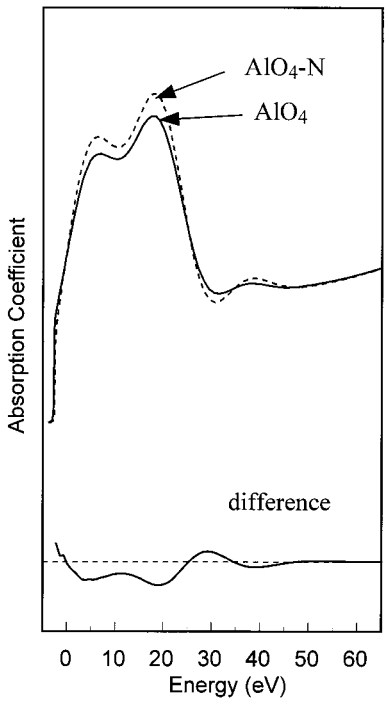

Figure 7. FEFF6 results for the AlK-edge on an AlO_4 cluster with an NH_4^+ ion and an Na^+ atom in the second shell. Also shown is the difference between these spectra.

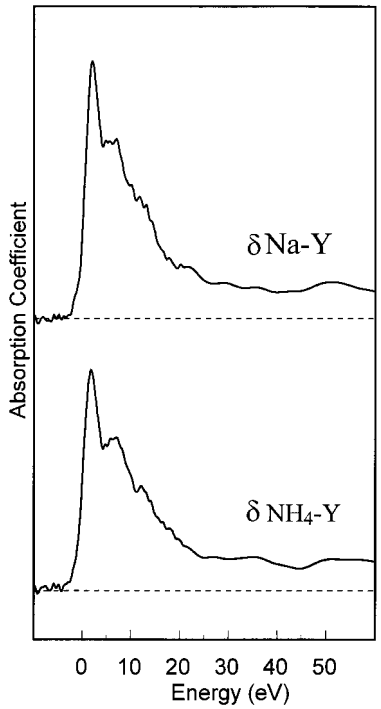

Figure 8. Zeolite difference spectra, δ (Na^+-Y) = (H^+-Y) − (Na^+-Y) and δ (NH_4^+-Y) = (H^+-Y) − (NH_4^+-Y), after renormalization on a tetrahedral atom basis of the H^+-Y spectrum as described in the text.

Interpretation of the Difference Spectra (dif. Na−Y, dif. NH_4−Y) in the Y Zeolite. A proper interpretation of the differences seen in the zeolite NEXAFS can be determined using ^{27}Al MAS NMR data. The ^{27}Al NMR data on the H^+-Y zeolite indicated the presence of 85% tetrahedrally coordinated and 15% octahedrally coordinated aluminum oxide, 98% tetrahedrally coordinated aluminum oxide for the NH_4^+-Y zeolite, and 100% for the Na^+-Y zeolite.[27] Based on these ^{27}Al MAS NMR data, we renormalized the H^+-Y zeolite spectrum on a tetrahedrally coordinated aluminum atom basis by multiplying the spectrum by a factor 100/85. This procedure is appropriate because the spectra were initially normalized on a per atom basis. Next, we performed a subtraction of this renormalized H^+-Y zeolite with the Na^+-Y and NH_4^+-Y zeolite, respectively. The spectra of Na^+-Y and NH_4^+-Y zeolite can be seen as characteristic for tetrahedrally coordinated aluminum oxide in the Y zeolite, as shown in Figure 3. In Figure 8 the two difference spectra are given:

$$\delta\ (Na^+-Y) = 100/85 \cdot (H^+-Y) - (Na^+-Y)$$

$$\delta\ (NH_4^+-Y) = 100/85 \cdot (H^+-Y) - (NH_4^+-Y)$$

To evaluate the influence of the multiplication factor on the resultant difference spectra we used different multiplication factors ranging from 100/75 to 100/95. The results (not shown) were spectra with basically similar shapes; only the relative amplitudes of the peaks showed minor changes. The results of these subtractions with varying normalization factors indicate that the features visible in the difference spectra, δ (Na^+-Y) and δ (NH_4^+-Y) in Figure 8, are realistic and can be attributed to the presence of octahedrally coordinated aluminum oxide in the H^+-Y, as we will show next.

In Figure 9, the renormalized (on a tetrahedral atom basis) spectra δ (Na^+-Y) and δ (NH_4^+-Y) are compared with the Na^+-Y zeolite spectrum. The energy range in Figure 9 is much less than that in Figure 8. The difference spectra are remarkably

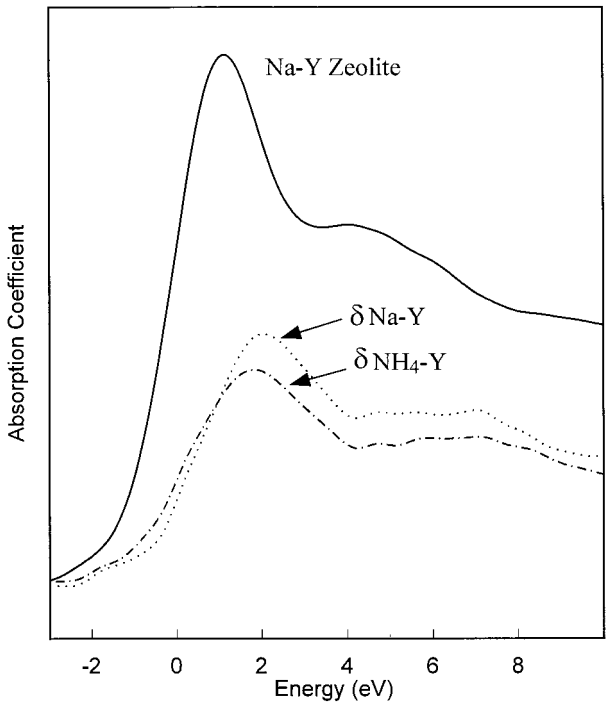

Figure 9. Comparison of the Na^+-Y spectra (reflecting 100% tetrahedral Al sites) with the δ difference spectra shown in Figure 8 (representing octahedral sites as interpreted in this work).

similar to each other, but different from the Na^+-Y. The Na^+-Y is 100% tetrahedrally coordinated Al, according to ^{27}Al MAS NMR. The whitelines in the difference spectra are shifted to higher energy in comparison with the whiteline of the Na^+-Y, a characteristic difference between spectra of octahedrally and tetrahedrally coordinated compounds (Table 1).

In Figure 10, δ (Na^+-Y) and δ (NH_4^+-Y) are compared with the experimental spectrum of corundum (a compound with

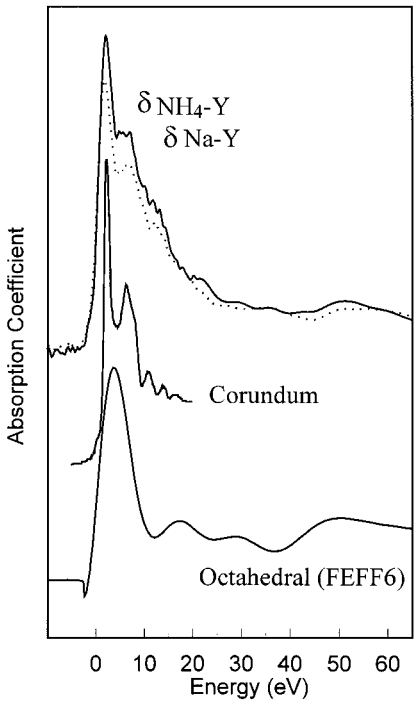

Figure 10. Comparison of the zeolite δ difference spectra with the experimental AlK-edge NEXAFS data for corundum and FEFF6 results for octahedrally coordinated Al.

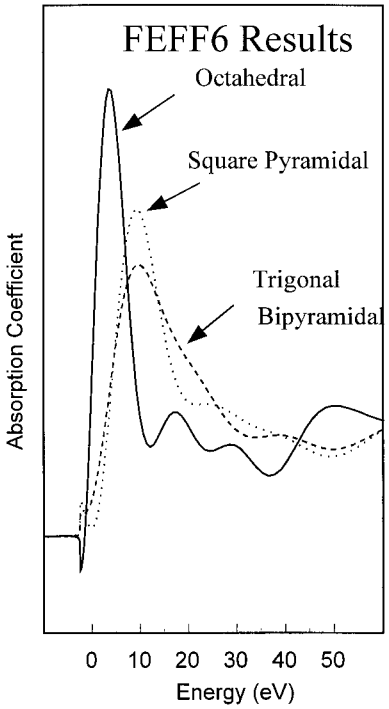

Figure 11. Comparison of FEFF6 results for octahedral aluminum with Al−O bond length of 1.85 Å with square pyramidal and trigonal bipyramidal coordination, both having Al−O bond lengths of 1.70 Å.

Al in a distorted octahedral conformation). For comparison, an FEFF6 calculation on an AlO_6 cluster with the Al octahedrally coordinated and with an Al−O bond length of 1.85 Å is also shown. The whiteline in the δ spectra is split by ~4 eV, which is equal to the splitting in the spectra of compounds with distorted octahedral symmetry. Furthermore, the difference spectra show a peak at ~50 eV, which coincides with a peak in the FEFF6 calculated spectrum. In Table 1, we recognized this peak to be a sensitive measure of the Al−O bond length. In addition, it can be seen that the whiteline has a large intensity compared with the intensity at high energy (arbitrarily 45 eV above threshold). All these features, including the shift in whiteline, indicate that the difference spectrum can be attributed to distorted octahedrally coordinated aluminum oxide with a bond length in the range 1.85−1.90 Å, as indicated by the 50 eV peak.

Although the similarities are evident, there are some distinct differences visible in the difference spectra and the corundum spectra (or for any other distorted octahedral compound). These differences cannot be explained either by the presence of a cation or by differences in bond length distances. This difference is a surplus of intensity around 10 to 15 eV above threshold in the difference spectra compared with a spectrum of a distorted octahedrally coordinated compound, as well as poorer resolution of the 1568 and 1572 eV peaks compared with standard compounds.

We can give two possible interpretations for these noted differences. The surplus in intensity around 10−15 eV might indicate the presence of pentacoordinated Al. Figure 11 shows FEFF6 calculations on pentacoordinated Al. The aluminum oxygen bond length for these calculations is 1.70 Å. For comparison, a calculated spectrum for an octahedrally coordinated AlO_6 cluster with an aluminum oxygen bond length of 1.90 Å is added. Two possible conformations (trigonal bipyramidal and square pyramidal) of pentacoordinated Al both show high intensity in the 10−15 eV range, which might indicate the presence of one of these two conformations. Moreover, when taking the difference between the δ spectra and the corundum spectrum, a whiteline is found that falls exactly between the whitelines of the octahedrally and tetrahedrally coordinated Al. The position of this whiteline is another possible indication for the presence of these pentacoordinated species.

However, a second more likely interpretation is possible. It is likely that the octahedrally coordinated Al in the H^+−Y zeolite is present in small Al_2O_3 clusters, or even as isolated ions.[5] Moreover, recently, octahedral Al has been proposed to be positioned in the framework of the acidic zeolite Y.[28] The octahedral Al observed here could be this aluminum. As already discussed, the features in the 10−15 eV range are determined by intermediate- and long-range order, which might not be fully present in these small clusters. Cabaret et al.[22] show in their calculations of increasing cluster size that the fine structure features get increasingly resolved as the cluster size increases. The poorly resolved peaks at 1568 and 1572 eV in the distorted octahedral Al in the H^+−Y zeolite might be a fingerprint for the lack of long-range ordering.

Conclusions

NEXAFS data has proven to be a successful tool in providing unique geometrical information on Al coordination. The Al NEXAFS spectra of various minerals and Y zeolites are interpreted successfully starting at ~15 eV above threshold using the curved-wave multiple-scattering cluster calculations performed in FEFF6. Characteristic features for the different conformations are identified. Using several criteria it is possible to distinguish octahedrally (distorted or not), tetrahedrally, and square planar coordinated aluminum. It is also shown that mixed coordinations can be separated and identified.

A distorted octahedral conformation could be distinguished from a regular octahedral conformation. It is further indicated that the fine structure just above the edge is determined by medium- and long-range order, whereas the resonances at higher energy (20 eV) are determined by several multiple-scattering

paths in the first shell. Finally, at still higher energies, single EXAFS scattering features exists. These peaks give a clear indication of the Al−O bond length, as well as the shape resonances at the somewhat lower energies.

Using the established characteristic features in the NEXAFS line shapes for each coordination geometry, separate contributions to the NEXAFS line shape of the H^+−Y zeolite could be identified. In addition to the tetrahedral conformation, the presence of distorted octahedrally coordinated Al could be assigned. The relative intensities of the contributions correspond to ∼90% for the tetrahedral and 10% for the octahedral Al.

Acknowledgment. This work was supported by the Office of Naval Research (USA), by the Catalysis Center Utrecht (NL), and by the Technology Foundation and was carried out in connection with Netherlands Institute for Catalysis Research NIOK. The authors thank H. Qian and T. Nabi for their interesting and helpful discussions.

References and Notes

(1) Bahtia, S. *Zeolite Catalysis: Principles and Applications*, CRC: Boca Raton, FL, 1990; pp 1−5.

(2) Meir, V. M. *Molecular Sieves*; Soc. Chem. Ind.: London, 1968.

(3) Smith, J. V. *Zeolite Chemistry and Catalysis*; Rabo, J. A., Ed.; ACS Monograph, 1976; p 171.

(4) Fyfe, C. A.; Mueller, K. T.; Kokotailo, G. T. *NMR Techniques in Catalysis*; Bell, A. T.; Pines, A., Eds.; Marcel Dekker: New York, 1994.

(5) Beyerlein, R. A.; Choi-Feng, C.; Hall, J. B.; Huggins, B. J.; Ray, G. J. *Top. Catalysis* **1997**, *4*, 27−42.

(6) Heald, S. M. *X-ray Absorption: Principles, Applications, Techniques of EXAFS, SEXAFS and XANES*; Koningsberger, D. C.; Prins, R., Eds.; Wiley: New York, 1988; pp 87−118.

(7) Koningsberger, D. C.; Miller, J. T. *Catal. Lett*. **1994**, *29*, 77−90.

(8) van Bokhoven, J. A.; Sambe, H.; Koningsberger, D. C.; Ramaker, D. E. *J. Phys. IV France* **1997**, *7*, Colloque C2 (Supplément au Journal de Physique III d'Avril, **1997**, C2−835−840).

(9) Heald, S. M. *X-ray Absorption: Principles, Applications, Techniques of EXAFS, SEXAFS and XANES*; Koningsberger, D. C.; Prins, R., Eds.; Wiley: New York, 1988; p 87.

(10) Cook, J. W., Jr.; Sayers, D. E. *J. Appl. Phys.* **1981**, *52*, 5024.

(11) DeLeon, J. M.; Rehr, J. J.; Zabinsky, S. I.; Albers, R. C. *Phys. Rev. B: Condens. Matter* **1991**, *44*−*9*, 4146−4156.

(12) Rehr, J. J. *J. Appl. Phys. Supp.* **1993**, *32*−*2*, 8−12.

(13) Sambe, H.; Qian, X.; Ramaker, D. E. *Phys. Rev. B: Condens. Matter* **1996-II**, *53*, *4*, 1770−1782.

(14) Qian, X.; Sambe, H.; Ramaker, D. E. *Phys. Rev. B*: *Condens. Matter* **1995**, *52*, 15115−15121.

(15) Landron, C.; Badets, M. C.; Douy, A.; Coutures, J.; Coutures, J. P.; Daniel, P.; Flank, A. M. *Phys. Stat. Sol.* **1991**, *167*, 429−440.

(16) Wyckoff, R. W. G. *Crystal Structure*, Vol. 1, 2nd ed.; John Wiley and Sons: New York, 1963; p 7.

(17) Waychunas, G. A.; Brown, G. E., Jr. *EXAFS and Near Edge Structures III*; Hodgts, K. A.; Hedman, B.; Penner-Hahn, J. E., Eds.; Springer-Verlag: Berlin, 1984; pp 336−342.

(18) Li, D.; Bancroft, G. M.; Fleet, M. E.; Feng, X. H.; Pan, Y. *Am. Miner*. **1995**, *80*, 432−440.

(19) McKeown, D. A.; Waychunas, G. A.; Brown, G. E., Jr. *J. Non-Cryst. Solids* **1985**, *74*, 349−371.

(20) Ildefonse, Ph.; Kirkpatrick, R. J.; Montez, B.; Cala, G.; Flank, A. M.; Lagrade, P. *Clays Clay Miner*. **1994**, *42(3)*, 276−287.

(21) Bugaev, L. A.; Ildefonse Ph.; Flank, A.-M.; Sokolenko, A. P.; Dmitrienko, H. V. *J. Phys.: Condens. Matter* **1998**, *10*, 5463−5473.

(22) Cabaret, D.; Sainctavit, Ph.; Ildefonse, Ph.; Flank, A.-M. *J. Phys.: Condens. Matter* **1996**, *8*, 3691−3704.

(23) Natoli, C. R.; Mimeser, D. K.; Donich, S. *Phys. Rev. A* **1980**, *22*, 1104−1108.

(24) Nonpublished data.

(25) Dodelet, J. P.; Tourillon, G.; Gastonguay, L.; Côté, R.; Guay, D.; Ladouceur, M.; Flank, A.-M.; Lagarde, D. *J. Phys. Chem*. **1992**, *96*, 7202−7206.

(26) Kamijo, N.; Kageyama, H.; Kaeabata, K.; Nishihagi, L.; Uehara, Y.; Taniguchi, K. *EXAFS and Near Edge Structures III*; Hodgts, K. A.; Hedman, B.; Penner-Hahn, J. E., Eds.; Springer-Verlag: Berlin, 1984; pp 613−615.

(27) Theunissen, E. H.; van Santen, R. A.; Jansen, A. P. J.; van Duijneveldt, F. B. *J. Phys. Chem*. **1993**, *97*, 203−210.

(28) Koningsberger, D. C.; Miller, J. T. *Studies in Surface Science and Catalysis*, Vol. 101; Hightower, J. W.; Delgass, W. N.; Iglesia, E.; Bell, A. T., Eds.; Elsevier: Amsterdam, 1996; pp 841−850.

(29) Wouters, B. H.; Chen, T.-H.; Grobet, P. J. *J. Am. Chem. Soc*. **1998**, *120*, 11419−11425.